Publ. Astron. Soc. Japan (2021) 73 (1), 25–43
doi: 10.1093/pasj/psaa110
Advance Access Publication Date: 2021 January 22

Follow-up observations for IceCube-170922A: Detection of rapid near-infrared variability and intensive monitoring of TXS 0506+056

Tomoki Morokuma [1,*] Yousuke Utsumi [2] Kouji Ohta [3] Masayuki Yamanaka [4] Koji S. Kawabata [5] Yoshiyuki Inoue [6,7,8] Masaomi Tanaka [9] Michitoshi Yoshida [10] Ryosuke Itoh [11] Mahito Sasada [5] Nozomu Tominaga [12,8] Hiroki Mori [13] Miho Kawabata [3] Tatsuya Nakaoka [5] Maiko Chogi [13] Taisei Abe [13] Ruochen Huang [13] Naoki Kawahara [13] Hiroki Kimura [13] Hiroki Nagashima [13] Kengo Takagi [13] Yuina Yamazaki [13] Wei Liu [14,15,5] Ryou Ohsawa [1] Shigeyuki Sako [1] Katsuhiro L. Murata [16] Kumiko Morihana [17,18] Christina K. Gilligan [19] Keisuke Isogai [4] Mariko Kimura [3,20] Yasuyuki Wakamatsu [3] Ryuhei Ohnishi [3] Masaki Takayama [21] Satoshi Honda [21] Yoshiki Matsuoka [22] Takuji Yamashita [22,23] Shigehiro Nagataki [7,24] and Yasuyuki T. Tanaka [5]

[1]Institute of Astronomy, Graduate School of Science, The University of Tokyo, 2-21-1 Osawa, Mitaka, Tokyo 181-0015, Japan
[2]Kavli Institute for Particle Astrophysics and Cosmology, SLAC National Accelerator Laboratory, Stanford University, Menlo Park, CA 94025, USA
[3]Department of Astronomy, Graduate School of Science, Kyoto University, Kitashirakawa-Oiwake-cho, Sakyo-ku, Kyoto, Kyoto 606-8502, Japan
[4]Okayama Observatory, Kyoto University, 3037-5 Honjo, Kamogata-cho, Asakuchi, Okayama 719-0232, Japan
[5]Hiroshima Astrophysical Science Center, Hiroshima University, 1-3-1 Kagamiyama, Higashi-Hiroshima, Hiroshima 739-8526, Japan
[6]Department of Earth and Space Science, Graduate School of Science, Osaka University, 1-1 Machikaneyama, Toyonaka, Osaka 560-0043, Japan
[7]Interdisciplinary Theoretical & Mathematical Science Program (iTHEMS), RIKEN, 2-1 Hirosawa, Saitama 351-0198, Japan
[8]Kavli Institute for the Physics and Mathematics of the Universe (WPI), UTIAS, The University of Tokyo, 5-1-5 Kashiwanoha, Kashiwa, Chiba 277-8583, Japan
[9]Astronomical Institute, Tohoku University, Aramaki, Aoba-ku, Sendai, Miyagi 980-8578, Japan
[10]Subaru Telescope, National Astronomical Observatory of Japan, National Institutes of Natural Sciences, 650 North A'ohoku Place, Hilo, HI 96720, USA
[11]Bisei Astronomical Observatory, 1723-70 Okura, Bisei, Ibara, Okayama 714-1411, Japan
[12]Department of Physics, Faculty of Science and Engineering, Konan University, 8-9-1 Okamoto, Kobe, Hyogo 658-8501, Japan
[13]Graduate School of Advanced Science and Engineering, Hiroshima University, 1-3-1 Kagamiyama, Higashi-Hiroshima, Hiroshima 739-8526, Japan

[14]Purple Mountain Observatory, Chinese Academy of Sciences, No. 10 Yuanhua Road, Qixia District, Nanjing, 210023, China
[15]Key Laboratory for Radio Astronomy, Chinese Academy of Sciences, Nanjing 210008, China
[16]Department of Physics, Tokyo Institute of Technology, 2-12-1 Ookayama, Meguro-ku, Tokyo 152-8551, Japan
[17]Department of Astrophysics, Nagoya University, Chikusa-ku, Nagoya, Aichi 464-8602, Japan
[18]Institute of Liberal Arts and Sciences, Nagoya University, Furo-cho, Chikusa-ku, Nagoya, Aichi 464-8602, Japan
[19]Department of Physics and Astronomy, Dartmouth College, Hanover, NH 03784, USA
[20]Institute of Physical and Chemical Research (RIKEN), 2-1 Hirosawa, Wako, Saitama 351-0198, Japan
[21]Nishi-Harima Astronomical Observatory, Center for Astronomy, University of Hyogo, 407-2 Nishigaichi, Sayo-cho, Sayo, Hyogo 679-5313, Japan
[22]Research Center for Space and Cosmic Evolution, Ehime University, 2-5 Bunkyo-cho, Matsuyama, Ehime 790-8577, Japan
[23]National Astronomical Observatory of Japan, National Institutes of Natural Sciences, 2-21-1 Osawa, Mitaka, Tokyo 181-8588, Japan
[24]Astrophysical Big Bang Laboratory (ABBL), RIKEN Cluster for Pioneering Research, RIKEN, 2-1 Hirosawa, Wako, Saitama 351-0198, Japan

*E-mail: tmorokuma@ioa.s.u-tokyo.ac.jp

Received 2020 June 4; Accepted 2020 November 4

Abstract

We present our follow-up observations to search for an electromagnetic counterpart of the IceCube high-energy neutrino IceCube-170922A. Monitoring observations of a likely counterpart, TXS 0506+056, are also described. First, we quickly took optical and near-infrared images of seven flat-spectrum radio sources within the IceCube error region right after the neutrino detection and found a rapid flux decline of TXS 0506+056 in Kanata/HONIR *J*-band data. Motivated by this discovery, intensive follow-up observations of TXS 0506+056 were continuously performed, including our monitoring imaging observations, spectroscopic observations, and polarimetric observations in optical and near-infrared wavelengths. TXS 0506+056 showed a large-amplitude (∼1.0 mag) variability in a time scale of several days or longer, although no significant variability was detected in a time scale of a day or shorter. TXS 0506+056 also showed a bluer-when-brighter trend in optical and near-infrared wavelengths. Structure functions of the variabilities were examined and indicate that TXS 0506+056 is not a special blazar in terms of optical variability. Polarization measurement results of TXS 0506+056 are also discussed.

Key words: BL Lacertae objects: general — BL Lacertae objects: individual (TXS 0506+056) — galaxies: active — neutrinos — relativistic processes — surveys

1 Introduction

Recent detections of high-energy, TeV–PeV, neutrinos realized by the IceCube experiment (Aartsen et al. 2014) have made more exciting the electromagnetic identification of the neutrino sources. Such high-energy neutrinos are produced by the decay of charged pions which are created through cosmic-ray interactions with radiation ($p\gamma$; Winter 2013) or gas (pp; Murase et al. 2013). Therefore, detection of high-energy neutrinos is smoking-gun evidence of the existence of high-energy protons (cosmic rays). Observations of high-energy neutrinos provide unique information about cosmic-ray acceleration mechanisms and their acceleration sites, if their origins are identified.

In IceCube Collaboration (2015), detections of a total of 54 neutrino events by the IceCube experiment are reported from data covering 4 years. The arrival directions of the 54 IceCube events are consistent with being isotropic and do not show any clustering in the Galactic plane (IceCube Collaboration 2015), indicating that the neutrino sources would be extragalactic (Aartsen et al. 2014). Neutrinos can

travel cosmological distances without being deflected by cosmic magnetic fields or absorbed by photon fields. On the other hand, the contribution of high-redshift sources represents only a small fraction of the total observed flux due to redshift dilution. Thus, the competition between the neutrino's penetrating power and the redshift dilution makes emissions from sources at redshifts of $z \sim 1$–2 dominant in IceCube single-neutrino (*singlet*) events (Kotera et al. 2010; Icecube Collaboration 2017). The IceCube collaboration started issuing real-time alerts in 2016 April (Aartsen et al. 2017c), and the number of neutrino detections is increasing.

Many hypotheses for the origin of high-energy neutrinos have been proposed, including blazars (Mannheim 1995; Mücke et al. 2003; Becker et al. 2005), starburst galaxies (Loeb & Waxman 2006; Bechtol et al. 2017), Type IIn supernovae (Murase et al. 2011; Aartsen et al. 2015), choked-jet supernovae (Razzaque et al. 2004; Senno et al. 2016), gamma-ray bursts (GRBs; Waxman & Bahcall 1997; Aartsen et al. 2017b), tidal disruption events (TDEs; Senno et al. 2017), and active galactic nuclei (AGNs) core (Eichler 1979; Inoue et al. 2019).

Attempts have been made to assess these theories observationally, and some observational results set constraints on the theories as described in the this paragraph. Kadler et al. (2016) showed that a high-fluence GeV blazar, PKS 1424−418, is a possible origin for one of the high-energy starting events (HESEs), HESE-35, based on the temporal and positional coincidence between the neutrino detection and the γ-ray flare of the blazar. This blazar shows broad C IV, C III, and Mg II lines in its optical spectrum and is classified as a flat-spectrum radio quasar (FSRQ) at $z = 1.522$ (White et al. 1988). On the other hand, there is not, in general, good spatial and temporal correlation between neutrino detections and Fermi γ-ray blazars, indicating that the contribution of Fermi γ-ray blazars to the diffuse neutrino flux is as small as <27% (Aartsen et al. 2017a). No other origin candidates have been strongly supported as a significantly contributing source to the neutrino background (Senno et al. 2016, 2017; Bechtol et al. 2017). Very recently, a radio-emitting TDE at $z = 0.051$, discovered on 2019 April 1, was claimed to be an associated source to the neutrino event IceCube-191001A (Stein et al. 2020).

On 2017 September 22 at 20:54:30.43 (MJD = 58018.871), the IceCube experiment detected a track event of a high-energy neutrino (∼290 TeV; IceCube Collaboration 2018), IceCube-170922A, and Kopper and Blaufuss (2017) reported it via the Gamma-ray Coordinates Network (GCN) Circular. The direction was constrained to be RA $= 77.^{\circ}43^{+0.95}_{-0.65}$ and Dec $= +5.^{\circ}72^{+0.50}_{-0.30}$ in J2000.0 equinox (90% confidence region). TXS 0506+056, a BL Lac blazar within the error region, was pointed out to be a good candidate for the counterpart (Tanaka et al. 2017; see also subsection 3.1) and was subsequently observed with many telescopes over a wide wavelength range (IceCube Collaboration 2018). During the intensive follow-up observations, the redshift of TXS 0506+056 was successfully determined to be $z = 0.3365$ (Paiano et al. 2018). In addition, TXS 0506+056 was independently detected in high-energy γ-ray with the Large Area Telescope (LAT) on the Fermi satellite (Tanaka et al. 2017; IceCube Collaboration 2018), the MAGIC telescope (IceCube Collaboration 2018; Ansoldi et al. 2018), and the AGILE γ-ray telescope (Lucarelli et al. 2019), which strengthens the coincidence between TXS 0506+056 and the neutrino source.

TXS 0506+056 is a blazar registered in the Texas Survey of Radio Sources catalog (Douglas et al. 1996) and one of the highest-energy γ-ray-emitting blazars among those detected by the Energetic Gamma Ray Experiment Telescope (EGRET) γ-ray (30 MeV–30 GeV) satellite (Dingus & Bertsch 2001). The radio-to-gamma-ray spectral energy distribution (SED; IceCube Collaboration 2018) in combination with its featureless spectra (Paiano et al. 2018; IceCube Collaboration 2018) and peak frequency ν_S of $10^{14.5 \pm 0.25}$ Hz (Padovani et al. 2019) indicate that TXS 0506+056 is an intermediate synchrotron peaked ($10^{14} < \nu_S < 10^{15}$ Hz) BL Lac object (ISP or IBL; Padovani et al. 2018), although Padovani et al. (2019) claimed that TXS 0506+056 is a masquerading BL Lac. The bolometric luminosity $L_{\rm bol}$ is estimated to be a few $\times$ 10^{45} erg s^{-1} (Padovani et al. 2019), which is roughly consistent with being an ISP by following the so-called blazar sequence (Fossati et al. 1998; Kubo et al. 1998; Ghisellini et al. 2017).

In BL Lac SEDs, non-thermal emission from a relativistic jet dominates the thermal emission from an accretion disk in rest-frame UV-optical wavelengths and from a dusty torus in rest-frame near-infrared (NIR) wavelengths, as well as its host galaxy. Temporal flux (luminosity) variability of blazars is sometimes explained by a shock-in-jet model (Marscher & Gear 1985), and it is useful to see a possible link between neutrino emission, probably from a relativistic jet, and electromagnetic emission activities. To assess whether or not TXS 0506+056 is a special blazar and 2017 September 22 is a special timing, it is worth examining the variability properties of TXS 0506+056. Blazars, in general, show large and rapid variability in optical wavelengths (Bauer et al. 2009), which could be a key to understanding the relationship with neutrino emission. Although it is dependent on blazar types, intranight variability is significantly detected for several tens of percent of blazars, and its duty cycles are also several tens of percent (Rani et al. 2011; Paliya et al. 2017; Bachev et al. 2017; Gaur et al. 2017). Thus, short-time-scale variability is also

worth examining. Polarization information would also provide clues to understanding what happens in a relativistic jet.

The structure of this paper is as follows. In section 2 we describe our follow-up observations after the IceCube-170922A alert, including imaging and spectroscopic observations in the optical and near-infrared wavelengths. We describe and discuss the observational results in section 3. The neutrino direction and TXS 0506+056 are inside the Pan-STARRS1 (PS1; Chambers et al. 2016) footprint and outside the Sloan Digital Sky Survey (SDSS; York et al. 2000) footprint. The cosmological parameters used in this paper are $\Omega_M = 0.3$, $\Omega_\Lambda = 0.7$, $H_0 = 70\,\mathrm{km\,s^{-1}\,Mpc^{-1}}$. All the observing times are specified in UT.

2 Follow-up observations and data reduction

We started intensive follow-up observations in optical and NIR wavelengths right after receiving the real-time alert of the event. In this section we summarize our general strategy for identifying an electromagnetic counterpart of an IceCube neutrino-emitting source (subsection 2.1), quick observations to search for a IceCube-170922A counterpart candidate (subsections 2.2 and 2.3), and follow-up observations after a likely counterpart, TXS 0506+056, was identified, including monitoring imaging and spectroscopic observations. Polarimetric observations for TXS 0506+056 are also described (subsection 2.4).

2.1 Strategy for seeking an IceCube-170922A electromagnetic counterpart

Since the real-time alert system of IceCube was started in 2016 April (Aartsen et al. 2017c), we have organized a strategic optical and NIR follow-up observing group utilizing the Optical and Infrared Synergetic Telescopes for Education and Research (OISTER; M. Yamanaka et al. in preparation) and other Japanese facilities. Considering multiple possibilities for transient high-energy neutrino sources, we adopt multiple observing strategies using our optical and NIR facilities.

In order to test the blazar scenario, we first select blazar candidates with flat radio spectra catalogued in the BROS catalog (Itoh et al. 2020). The BROS catalog collects flat-spectrum radio sources selected using a combined catalog (de Gasperin et al. 2018) of the National Radio Astronomy Observatory Very Large Array Sky Survey (NVSS; Condon et al. 1998; 1.4 GHz) and the Tata Institute of Fundamental Research Giant Metrewave Radio Telescope Sky Survey (TGSS; Intema et al. 2017; 150 MHz) catalogs. The final criterion on the radio spectral slope to select flat-spectrum objects is $\alpha > -0.6$ where $f_\nu \propto \nu^\alpha$ (Itoh et al. 2020), while the criterion was $\alpha > -0.5$ at the observation times in this paper. We carry out optical and NIR imaging observations to detect any possible brightness change from a neutrino-emitting blazar within an IceCube localization. For this purpose, 1–2 m class telescopes in the OISTER collaboration are mainly used. A fraction of the BROS sources are apparently optically faint and not detected in the PS1 data. We search for variabilities of such faint blazar candidates with Hyper Suprime-Cam (HSC; Miyazaki et al. 2012) on the 8.2 m Subaru telescope.

Supernovae are also thought to be candidates for generating high-energy neutrinos. To find a supernova from which a neutrino may originate, we also carry out wide-field optical imaging surveys to cover a significant fraction of an IceCube localization using wide-field optical imagers such as the Kiso Wide Field Camera (KWFC; Sako et al. 2012)[1] and Tomo-e Gozen (Sako et al. 2016, 2018) on the 1.05 m Kiso Schimidt telescope and HSC on the 8.2 m Subaru telescope.

For the IceCube-170922A event, we performed optical and NIR observations with both these strategies. Our blind survey for supernovae is described in a separate paper (T. Morokuma et al. in preparation).

2.2 Optical and NIR imaging

All the imaging observations are summarized below and in table 1. The detailed characteristics of the telescopes and instruments are summarized in the table.

2.2.1 Initial response to the alert: Search for a rapidly variable blazar

We started follow-up imaging observations 0.8 d after the IceCube-170922A alert with the Hiroshima Optical and Near-Infrared camera (HONIR; Akitaya et al. 2014) on the 1.5 m Kanata telescope at the Higashi Hiroshima Observatory (R_C and J bands) and the KWFC (Sako et al. 2012) on the 1.05 m Kiso Schmidt telescope (g, r, and i bands). On subsequent nights, the HSC (Miyazaki et al. 2012) on the 8.2 m Subaru telescope (z band) and 0.5 m MITSuME Akeno telescope (Kotani et al. 2005; Yatsu et al. 2007; Shimokawabe et al. 2008; g, R_C, and I_C bands) were also used. The fields-of-view of KWFC and HSC are well suited to effectively covering the localization area given by IceCube, as shown in figure 1.

The brightness of a counterpart is unknown and difficult to predict because of the unknown nature of and distance to the counterpart. Thus, we adopt multiple exposure times of 3–180 s as summarized in table 1.

There were seven flat-spectrum radio sources in a preliminary version of the BROS catalog within or right outside the 90% localization of IceCube-170922A, as shown

[1] KWFC was decommissioned in 2018 August.

Table 1. Telescopes and instruments used for follow-up imaging observations.*

Mode	Telescope	Aperture [m]	Instrument	FoV	Filter	t_{exp} [s]
M	Kyoto	0.4	—	18′ (rectangle)	V	60
SM	MITSuME (Akeno)	0.5	—	28′ (rectangle)	g, R_C, I_C	60
SM	Kiso	1.05	KWFC	2.°2 (rectangle)	g, r, i	10, 30, 60, 180
M	Kiso	1.05	Tomo-e Gozen	(39.′7 × 22.′4) × 4†	No	0.5
M	IRSF	1.4	SIRIUS	7.′7 (rectangle)	J, H, K	10
SM	Kanata	1.5	HONIR	6′ (diameter)	R_C, J	25–95 (R_C), 10–80 (J)
SM	Subaru	8.2	HSC	1.°5 (diameter)	z	3–5

*In the first column, S and M denote "survey" and "monitoring," respectively.
†When we took the Tomo-e Gozen data, the instrument was operating with a limited number of sensors (four) before the completion of the 84-sensor instrument in 2019.

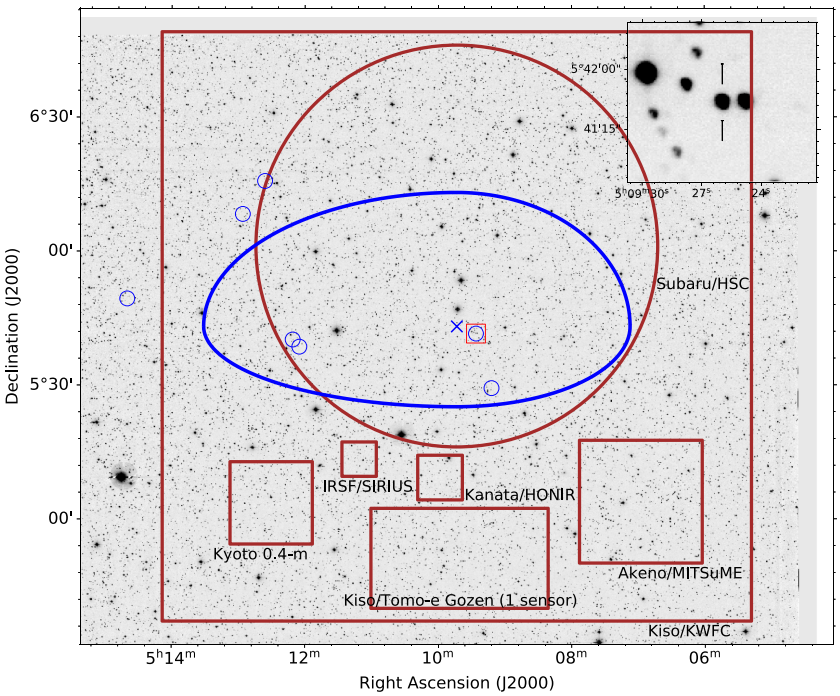

Fig. 1. Coadded *r*-band image of the field taken with KWFC. North is up and east is left. The IceCube 90% containment region (IceCube Collaboration 2018) is shown by the thick blue ellipse, and its center is indicated as a blue cross. The seven flat-spectrum radio sources in the preliminary BROS catalog which we observed first are indicated by small blue circles, and the TXS 0506+056 region is marked as a red rectangle, close to the blue cross. A zoomed-in 1′ × 1′ view around TXS 0506+056 is also shown in the top right inset. The fields of view of the optical and NIR instruments used in this paper are shown in brown. For Tomo-e Gozen, the field of view of one sensor is shown. (Color online)

in figure 1 and listed in table 2. Five of the seven sources were detected in the optical archival PS1 DR1 data. Each of the seven BROS sources was observed basically one by one with Kanata/HONIR and MITSuME, while all seven were also covered by two KWFC pointings and two HSC pointings. As described in subsection 3.1, we performed a quick data reduction for the data, and a Kanata/HONIR difference image for TXS 0506+056 revealed that it was fading on a time scale of a day.

2.2.2 Monitoring for TXS 0506+056

After detecting rapid NIR variability of TXS 0506+056 with Kanata/HONIR (described in subsection 3.1), we continued monitoring TXS 0506+056 with the telescopes described in sub-subsection 2.2.1. In addition, we carried out J-, H-, and K_s-band simultaneous imaging with SIRIUS (Nagayama et al. 2003; Nagayama 2012) on the 1.4 m Infrared Survey Facility (IRSF) and V-band imaging with the 0.4 m Kyoto telescope. The exposure times of the single images were 10 s and 60 s. We also took non-filter CMOS imaging data with Tomo-e Gozen (Sako et al. 2016, 2018) on the Kiso Schmidt telescope with the 2 fps readout mode. No filters were used; the sensors of Tomo-e Gozen are sensitive in ∼350–900 nm (Kojima et al. 2018).

2.2.3 Data reduction of imaging data

All the data were reduced in a standard manner, including bias, overscan, and dark current subtractions if necessary

Table 2. Seven flat-spectrum radio sources observed within or right outside the IceCube 90% error region.*

Name	RA, Dec (NVSS)	RA, Dec (PS1)	Sep.	$f_{\rm TGSS}$ [mJy]	$f_{\rm NVSS}$ [mJy]	r(PS1)	Note†
BROS J0509+0541	$05^{\rm h}09^{\rm m}26\overset{\rm s}{.}0$, $+05^\circ41'35\overset{''}{.}6$	$05^{\rm h}09^{\rm m}26\overset{\rm s}{.}0$, $+05^\circ41'35\overset{''}{.}4$	$4\overset{'}{.}58$	406.7	546.8	15.04	(1)
J0509+0529	$05^{\rm h}09^{\rm m}12\overset{\rm s}{.}0$, $+05^\circ29'22\overset{''}{.}0$	$05^{\rm h}09^{\rm m}12\overset{\rm s}{.}3$, $+05^\circ29'22\overset{''}{.}8$	$15\overset{'}{.}83$	25.8	17.9	17.05	(2)
BROS J0512+0538	$05^{\rm h}12^{\rm m}05\overset{\rm s}{.}7$, $+05^\circ38'41\overset{''}{.}7$	$05^{\rm h}12^{\rm m}05\overset{\rm s}{.}7$, $+05^\circ38'41\overset{''}{.}2$	$35\overset{'}{.}72$	57.9	24.0	15.95	
BROS J0512+0540	$05^{\rm h}12^{\rm m}11\overset{\rm s}{.}6$, $+05^\circ40'15\overset{''}{.}2$	$05^{\rm h}12^{\rm m}11\overset{\rm s}{.}6$, $+05^\circ40'15\overset{''}{.}6$	$37\overset{'}{.}03$	160.9	63.0	22.62	
J0512+0615	$05^{\rm h}12^{\rm m}36\overset{\rm s}{.}0$, $+06^\circ15'45\overset{''}{.}0$	$05^{\rm h}12^{\rm m}36\overset{\rm s}{.}6$, $+06^\circ15'43\overset{''}{.}8$	$54\overset{'}{.}03$	24.7	10.2	20.86	(2)
BROS J0512+0608	$05^{\rm h}12^{\rm m}56\overset{\rm s}{.}7$, $+06^\circ08'19\overset{''}{.}1$	$05^{\rm h}12^{\rm m}56\overset{\rm s}{.}8$, $+06^\circ08'17\overset{''}{.}6$	$54\overset{'}{.}28$	350.9	159.5	18.46	
BROS J0514+0549	$05^{\rm h}14^{\rm m}40\overset{\rm s}{.}1$, $+05^\circ49'23\overset{''}{.}2$	$05^{\rm h}14^{\rm m}39\overset{\rm s}{.}5$, $+05^\circ49'20\overset{''}{.}3$	$74\overset{'}{.}11$	267.6	268.0	19.87	

*These were registered in the preliminary version of the BROS catalog when we started the follow-up observations. The values are: coordinates of the sources in the NVSS and PS1 catalogs, separation from the IceCube detection center in arcmin, radio fluxes at 150 MHz (TGSS) and 1.4 GHz (NVSS) in mJy, and PS1 r-band Kron magnitude.

†Notes: (1) TXS 0506+056, FL8Y J0509.4+0542. (2) No objects in latest BROS.

and possible, flat-fielding, astrometry with optimistic pattern matching (OPM; Tabur 2007) or Astrometry.net (Lang et al. 2010), although some differences exist (e.g., distortion correction is applied only for HSC data). Details of the data reductions are described in Morokuma et al. (2014) for KWFC and Tachibana et al. (2018) for MITSuME. The HSC data were analyzed with hscPipe v4.0.5, which is the standard HSC reduction pipeline (Bosch et al. 2018). Tomo-e Gozen CMOS sensor data were also reduced with the dedicated pipeline described in Ohsawa et al. (2016).

Photometry was performed with SExtractor (Bertin & Arnouts 1996) using MAG_AUTO. All magnitudes in optical and NIR wavelengths are measured in the AB system. The optical magnitudes were calibrated relative to the PS1 Data Release 2 (DR2) catalog (Magnier et al. 2016; Flewelling et al. 2016). Johnson–Cousins filter data were also calibrated to PS1 data in filters with similar bandpasses (i.e., PS1 r for $R_{\rm C}$ and PS1 i for $I_{\rm C}$). No-filter Tomo-e Gozen data were also calibrated relative to r-band PS1 data. The magnitudes of field stars at NIR wavelengths were derived from the 2MASS database (Skrutskie et al. 2006) and converted to the AB system by following Tokunaga and Vacca (2005).

To search for a counterpart (sub-subsection 2.2.1), we applied an image subtraction method (Alard & Lupton 1998; Alard 2000) for the imaging data with reference images from PS1 in optical and 2MASS in NIR. Except for Subaru/HSC, all of our optical imaging data are shallower than PS1 images and the depths of the search are limited by the depths of our data. On the other hand, in NIR, 2MASS data are not so deep and we also performed another subtraction in which our first (reference) images were subtracted from our new data.

For photometry for the normal images without image subtractions, we add additional 3% errors to the errors measured with SExtractor. This is because photometry errors based on photon statistics usually underestimate the errors, which should follow a Gaussian distribution around the real values for non-variable objects, for example due to imperfect flat-fielding procedures.

2.2.4 ASAS-SN monitoring data

ASAS-SN covers a large fraction of the sky. Long-term data nicely covering before and after the neutrino detection are available, and significant variability and brightening of TXS 0506+056 before the neutrino detection were reported in Franckowiak et al. (2017). Original ASAS-SN V-band data are available and taken from ASAS-SN Sky Patrol[2] (Shappee et al. 2014; Kochanek et al. 2017). The data are calibrated relative to the AAVSO Photometric All-Sky Survey (APASS; Henden & Munari 2014). As mentioned in IceCube Collaboration (2018), the star nearby to the west,[3] $g_{\rm MeanPSF} = 14.7782 \pm 0.0024$, $r_{\rm MeanPSF} = 14.4373 \pm 0.0010$ in the PS1 DR2 catalog, corresponding to $V = 14.587$, which is converted using an equation in Kostov and Bonev (2018), contaminates the target flux in photometry of ASAS-SN Sky Patrol because of the coarse spatial sampling ($8''$ pixel^{-1}) and large PSF ($\sim 15''$ full width at half maximum) of ASAS-SN. We estimate the contribution to TXS 0506+056 to be 30% of the nearby star flux, and subtracted this from the target flux to extract only the flux of TXS 0506+056. We did not add additional errors to the original error of TXS 0506+056. We also confirmed that this correction does not change our conclusions. The brightness of the star nearby to the west is confirmed to be almost constant over our observing period based on our data.

[2] ⟨https://asas-sn.osu.edu⟩.

[3] Separated by $17\overset{''}{.}079$, objID = 114830773534352391, (RA, Dec) = ($05^{\rm h}09^{\rm m}24\overset{\rm s}{.}82$, $+05^\circ41'35\overset{''}{.}7$) in PS1 DR2.

Table 3. Telescopes and instruments used for follow-up spectroscopic observations.

Telescope	Aperture	Instrument	Grism	Filter	λ [Å]*	$R^{\dagger}$	$t_{\rm exp}$ [s]	Date (UT)	MJD
Nayuta	2.0 m	MALLS	150 l mm^{-1}	WG320	4700–8600	600	900 × 6	2017-09-29	58025.7
Kanata	1.5 m	HOWPol	grism	NONE	4700–9200	400	900 × 3	2017-09-29	58025.7
Subaru	8.2 m	FOCAS	300B	SY47	4600–8200	400	100 × 11	2017-09-30	58026.6
Subaru	8.2 m	FOCAS	VPH850	SO58	7500–10500	1200	100 × 7	2017-10-01	58027.6
Gemini-North	8.2 m	GMOS	B1200	NONE	3400–4960	3700	600 × (3 + 8) + 240 × 1	2017-11-11,15	58071.5

*Usable wavelength ranges rather than observed wavelength ranges.
†Spectral resolutions.

2.3 Optical spectroscopy

An obstacle to studying the neutrino source in detail was uncertain redshift determination of TXS 0506+056. Redshift determination of BL Lac objects is in general difficult and requires a large amount of observing time with a large-aperture optical telescope (Landoni et al. 2015a, 2015b) even if their images can be easily taken with 1 m class telescopes. This was the case for TXS 0506+056, and the redshift had not been reliably determined (Halpern et al. 2003).

TXS 0506+056 was spectroscopically observed in optical wavelengths, and the redshift is reported to be $z = 0.336$ in Ajello et al. (2014). However, the origin of this redshift determination is unclear from the figure and text in that paper. MAGIC high-energy γ-ray detection (Mirzoyan 2017, 2018) gives another constraint on the redshift through the measurement of the γ–γ attenuation effect. In IceCube Collaboration (2018), several conservative estimates were made with the MAGIC data, and the 95% confidence level upper limit on the source redshift was $z < 0.98$, while the lowest upper-limit redshift is $z < 0.41$. Since there were still debates on the redshift determination before Paiano et al. (2018) determined the redshift to be $z = 0.3365$, spectroscopic measurement was still important (Steele 2017; Morokuma et al. 2017).

We took optical long-slit spectra with the Medium And Low-dispersion Long-slit Spectrograph (MALLS) on the 2 m Nayuta telescope, HONIR (Akitaya et al. 2014) on the 1.5 m Kanata telescope, the Faint Object Camera and Spectrograph (FOCAS; Kashikawa et al. 2002) on the 8.2 m Subaru telescope, and the Gemini Multi-Object Spectrograph (GMOS; Hook et al. 2004) on the 8.2 m Gemini-North telescope. The spectral resolutions of the observations were mostly as low as $R \sim 1000$ or even lower. The exposure times were not so long, 1.5 hr at longest. These are summarized in table 3. The FOCAS observations and spectra are described and shown in the supplementary part of IceCube Collaboration (2018).

All the spectra were reduced in a standard manner with IRAF, including bias subtraction, flat-fielding, wavelength calibration, sky subtraction, and source extraction, while the Gemini-N/GMOS data was reduced with the Gemini IRAF package. Wavelength calibration was done using lamp spectra or night-sky lines. Flux calibration was not applied and the 1 d spectra obtained were normalized with continua to see any weak emission and absorption lines.

2.4 Optical and NIR polarimetry

We also conducted optical and NIR polarimetry observations with HONIR (Akitaya et al. 2014) at the Cassegrain focus on the 1.5 m Kanata telescope. HONIR is equipped with a rotatable half-wave plate and a Wollaston prism which enables us to conduct simultaneous polarimetry observations in optical and NIR channels. We used the R band and J band in the optical and NIR channels. The data were taken on 15 nights, from $t = 8$ d to $t = 213$ d after the IceCube alert. Each observation consisted of a set of four exposures at half-wave plate position angles of $0.^{\circ}0$, $22.^{\circ}5$, $45.^{\circ}0$, and $67.^{\circ}5$.

The data were reduced following the data analysis methodology described in Kawabata et al. (1999) to derive polarization degrees and angles. Instrumental polarization induced by the optical system within the Kanata telescope and HONIR has been confirmed to be as small as 0.1%–0.2% (Akitaya et al. 2014; Itoh et al. 2017).

Data taken with a fully polarizing filter inserted in front of HONIR were used for the correction of the wavelength-dependent origin points of the position angles (originating from the multi-layered superachromatic half-wave plate). The polarization degrees obtained were as stably high as $\gtrsim$99% with this filter in both R and J bands and we did not perform the depolarization correction. A strongly polarized star, BD $+64^{\circ}106$ (Schmidt et al. 1992), was observed to correct the observed position angle in celestial coordinates and was used to calibrate the position angles of TXS 0506+056. Galactic foreground polarization should be almost negligible ($P_R \lesssim 0.7\%$ or $P_J \lesssim 0.2\%$) because the interstellar extinction toward TXS 0506+056 is $A_R = 0.235$ or $A_J = 0.077$ mag (Schlafly & Finkbeiner 2011; Serkowski

et al. 1975). These values are mostly smaller than the measured values so we did not adopt any correction for the observed polarization.

The observing epochs are separated into two as below. The first epochs were ∼1.5 months after the IceCube alert. The second epochs were around $t \sim 180$ d after the alert, when larger polarization degrees of TXS 0506+056 based on polarimetric data taken with Liverpool/RINGO were reported (Steele et al. 2018). Motivated by this report, we also took additional polarization data with Kanata/HONIR.

3 Results and discussions

3.1 Discovery of rapid NIR variability of TXS 0506+056

We examined the subtracted *J*-band HONIR images (HONIR–HONIR and HONIR–2MASS) to see any rapid variability of the BROS blazars and blazar candidates. Figure 2 shows HONIR–HONIR subtraction images for the seven sources in table 2, which were listed in the preliminary BROS catalog at the observation time. We found that TXS 0506+056 showed a fading trend, by ∼0.15 mag, from 2017 September 23 to 24, as shown in the top panels of figure 2. In *g*-band data taken with Kiso/KWFC, about 0.15 mag decline was also detected. For the other sources, we did not find any significant NIR variability from the two-night HONIR data or did not detect the object, which was consistent with the non-detection or faint magnitudes recorded in the PS1 optical imaging data.

This rapid brightness change of TXS 0506+056 may indicate a possible relation with the neutrino detection, motivating examination of Fermi γ-ray all-sky monitoring data. One of the co-authors of this paper led this effort, found its γ-ray variability, and reported it via Astronomer's Telegram (ATel; Tanaka et al. 2017). This was further followed by multi-wavelength follow-up observations; see figure 3 and IceCube Collaboration (2018).

The timeline from the IceCube alert (Kopper & Blaufuss 2017) to the first Fermi ATel report (Tanaka et al. 2017) is summarized in figure 3. After the IceCube alert, some observational reports with monitoring and follow-up data were distributed via GCN and ATel. In summary, no possible related objects to the IceCube neutrino were mentioned in any of the reports before Tanaka, Buson, and Kocevski (2017). At the event time, no significant γ-rays (INTEGRAL SPI-ACS in Savchenko et al. 2017; HAWC in Martinez & Taboada 2017; H.E.S.S. in de Naurois & H.E.S.S. Collaboration 2017) or neutrinos (ANTARES in Dornic & Coleiro 2017a, 2017b), were detected. In Swift/XRT follow-up observations, nine sources were detected (including eight known sources; Keivani et al. 2017), although no special notices were made for TXS 0506+056.

3.2 Light curves of TXS 0506+056

Time variabilities of the observables are shown in figure 4 for optical magnitudes, NIR magnitudes, optical and NIR colors, optical and NIR polarization degrees and angles, and γ-ray fluxes in the low (100–800 MeV) and high (800 MeV–10 GeV) energy bands. In addition to our own data (subsection 2.2), optical *V*-band data from ASAS-SN (see sub-subsection 2.2.4), RINGO3 optical polarimetry data (see subsection 2.4), and Fermi γ-ray data were also used.

The γ-ray fluxes are taken from the Fermi All-sky Variability Analysis (FAVA; Abdollahi et al. 2017) website.[4] Aperture photometry fluxes in the low (100–800 MeV) and high (800 MeV–30 GeV) energy bands are used in this paper. We understand that the FAVA light curves are preliminary, as described on the FAVA website, but the temporal behavior is similar to those shown in IceCube Collaboration (2018) and the FAVA data are good enough for our purposes.

3.3 Variability of TXS 0506+056

We investigate optical and NIR variabilities in daily (sub-subsection 3.3.1), intranight (sub-subsection 3.3.2), and second-scale (sub-subsection 3.3.3) time scales. We construct structure functions (SFs) of the optical and NIR variability of TXS 0506+056, which are, in general, defined to be the ensemble variability of an object or a specific set of objects, to quantify its time variability. We compare the SFs of TXS 0506+056 with those of other AGNs in the literature. A caveat and problem are pointed out in Emmanoulopoulos, McHardy, and Uttley (2010) when an SF is used for studying the time scale of blazar variability; however, in this paper we discuss only the variability amplitudes at given time scales, not the time scale itself.

We adopt an usual concept in the definition of the structure function $V(\Delta t)$ as

$$V(\Delta t) = \sqrt{\langle |\Delta m|^2 \rangle - \langle \sigma_{S/N}^2 \rangle} \quad (1)$$

where Δt is the time interval between observations, Δm is the magnitude difference between different observations, and $\sigma_{S/N}$ is the measurement error in mag. We calculate SFs for TXS 0506+056 and neighboring stars with similar brightness to TXS 0506+056. These two SFs are compared

[4] ⟨https://fermi.gsfc.nasa.gov/ssc/data/access/lat/FAVA/⟩.

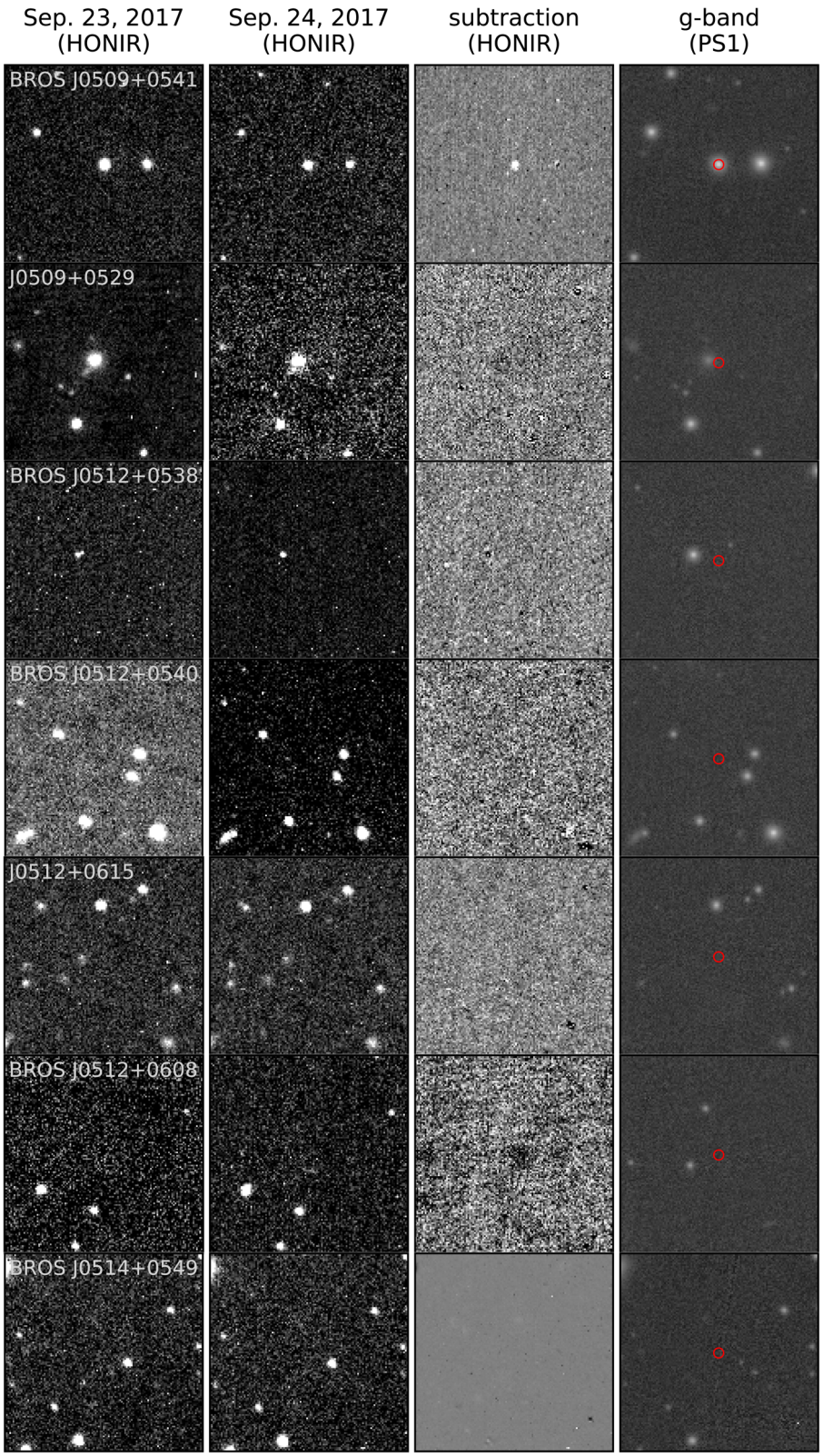

Fig. 2. HONIR *J*-band images and subtracted images for the seven flat-spectrum radio sources catalogued in the preliminary BROS when we started the follow-up observations (table 2). From left to right, HONIR *J*-band image on 2017 September 23, HONIR *J*-band image on 2017 September 24, subtracted HONIR *J*-band image (September 23–24), and PS1 *r*-band image are shown for each BROS source. The red circles on the PS1 images are NVSS radio locations with radii of 2″, which are typical positional errors of NVSS sources. (Color online)

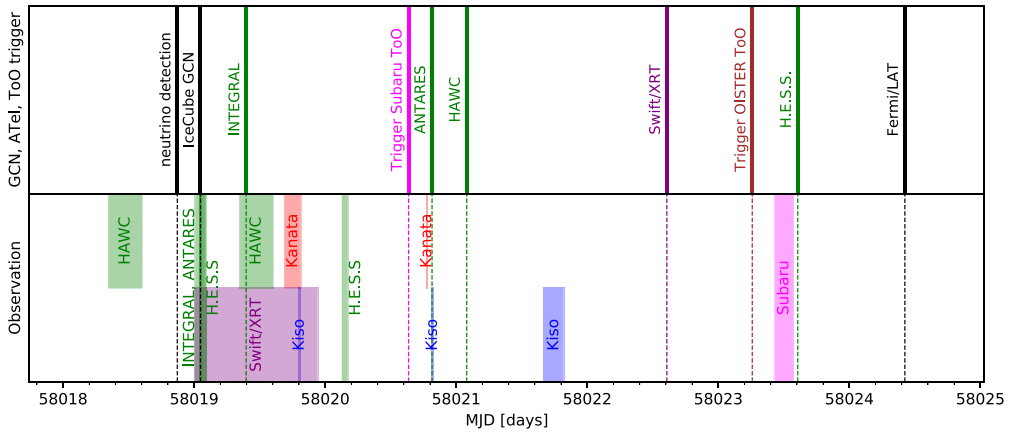

Fig. 3. Timeline of the follow-up observations from the IceCube alert. Kanata/HONIR, Kiso/KWFC, and Subaru/HSC observations are shown in red, blue, and magenta, respectively. The IceCube alert and the first GCN by (Tanaka et al. 2017) are indicated by solid black and green lines, respectively. (Color online)

to see any significant flux variability of TXS 0506+056. We estimate the median and 1σ confidence level with a bootstrap method.

The ASAS-SN data are useful for evaluating variability behavior before and around the alert, while our own data enable us to investigate short-time-scale variabilities after the alert.

The SFs obtained for TXS 0506+056 are shown in figure 5 and are compared with those of blazars (BL Lacs and FSRQs) studied in the Palomar-QUEST survey (Bauer et al. 2009), SDSS quasars (Vanden Berk et al. 2004), and CTA102 (Bachev et al. 2017). In Bauer et al. (2009), 94 BL Lacs, 278 FSRQs, and 4 marginally classified (BL Lacs or FSRQs) objects in total were observed with the 48 in Samuel Oschin Schmidt Telescope and QUEST2 Large Area Camera ($4.^{\circ}6 \times 3.^{\circ}6$ field-of-view; Baltay et al. 2007) over 3.5 years to construct the SFs shown in figure 5. In Vanden Berk et al. (2004), >25000 quasars were observed in the five optical bands (*ugriz*) and rest-frame (both in time scales and wavelengths) SFs derived, with different formulations but quantitatively equivalent to each other.

3.3.1 Long-term variability

Daily or longer time scale variability is summarized in this subsection. First, the optical and NIR fluxes are significantly variable, as shown in figure 4. The peak-to-peak amplitude reaches 1 mag. We also see some fluctuations over a time scale of a few days. In addition, none of the optical, NIR or γ-ray fluxes are at their peaks at the neutrino detection (IceCube Collaboration 2018). The overall trend around the neutrino detection indicates that TXS 0506+056 is in a declining phase. About 180 d after the neutrino detection, optical and NIR brightness increase again up to a brighter level than around the neutrino detection; however, no neutrino detection is reported in this period.

The optical SF amplitudes of TXS 0506+056 are comparable with or slightly larger than those of AGNs in the previous studies at time scales of $\Delta t > 10^1$ d. TXS 0506+056 is more variable by a factor of ∼2 than the SDSS quasars (Vanden Berk et al. 2004). The SFs of TXS 0506+056 in our measurements are larger than or comparable to those of FSRQs and BL Lacs (Bauer et al. 2009) at their face values. Note that the SFs of AGNs in general have 0.1 dex or larger scatter (Vanden Berk et al. 2004; Bauer et al. 2009), which make the envelope of the distribution overlap between those of FSRQs and BL Lacs and our measurements.

For NIR variability, TXS 0506+056 in the *J* band over time scales from a few days to a few tens of days, and *H* and K_s bands over a time scale of a few tens of days, are significantly more variable than neighboring stars. The NIR variabilities of TXS 0506+056 are as large as the optical ones in these time scales. The NIR variabilities at shorter time scales than a few days are comparable to those of neighboring stars and are almost at the limit of the measurement errors. Typical NIR variabilities of blazars in the literature are ∼0.1 mag (Sandrinelli et al. 2014; Li et al. 2018), which is comparable to our measurement for TXS 0506+056, and this variability behavior of TXS 0506+056 is not special.

We also calculated SFs using the ASAS-SN *V*-band data for each 30 d period from MJD = 57793 (225 d before the neutrino detection) to MJD = 58243 (225 d after the neutrino detection), covering the IceCube neutrino detection time on MJD ∼ 58018.87. The variability amplitudes for three time scales (1 d, 5 d, and 10 d) are derived from the SFs and shown in the fourth panel of figure 4. As a whole, there are no special periods when significantly larger variability is detected than other periods. It is not clear, but

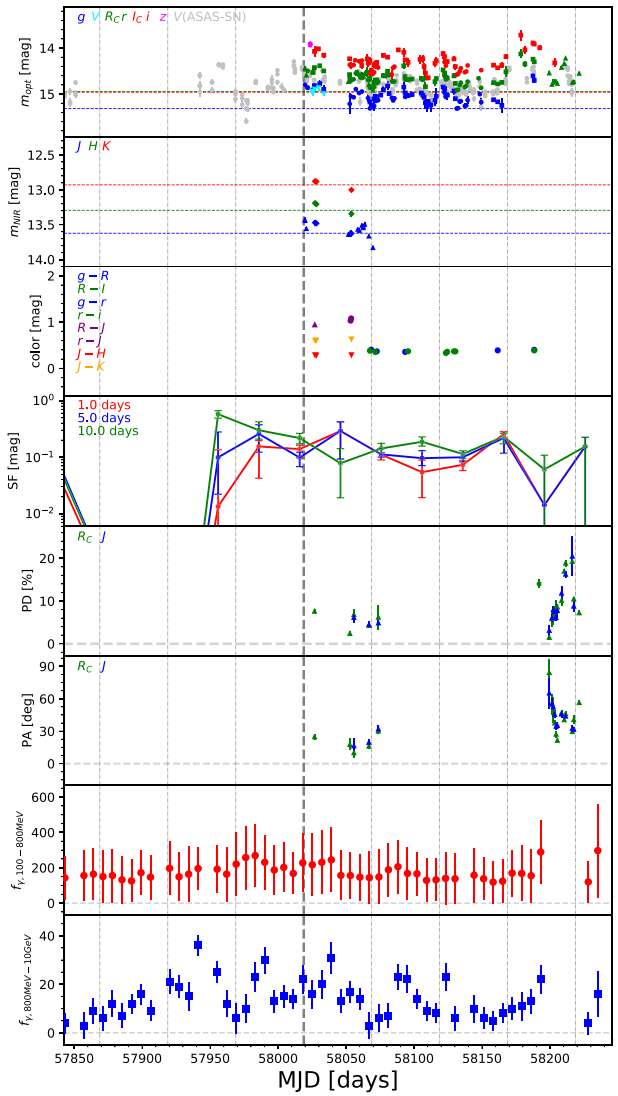

Fig. 4. Daily variabilities of optical (*g*, blue; *V*, cyan; *V* by ASAS-SN, gray; *R* and *r*, green; *I* and *i*, red; *z*, magenta) and NIR (*J*, blue; *H*, green; *K*, red) fluxes and optical–NIR colors from the top to the third panel. Changes of the structure functions in time scales of 1.0 d, 5.0 d, and 10.0 d are shown in the fourth panel. Daily changes of polarization degree (*R*, green; *J*, blue), polarization angle (*R*, green; *J*, blue), and Fermi/LAT γ-ray fluxes in the 200–800 MeV and 800 MeV–10 GeV energy bands are shown from the fifth to the bottom panel. For polarization degree, Liverpool/RINGO3 data is plotted in open circles (MJD $\sim$ 58192). The neutrino detection time is indicated as gray dashed vertical lines. Vertical dash-dotted gray lines indicate −150, −100, −50, +50, +100, +150, +200 d with respect to the IceCube neutrino detection. Galactic extinction is not corrected. (Color online)

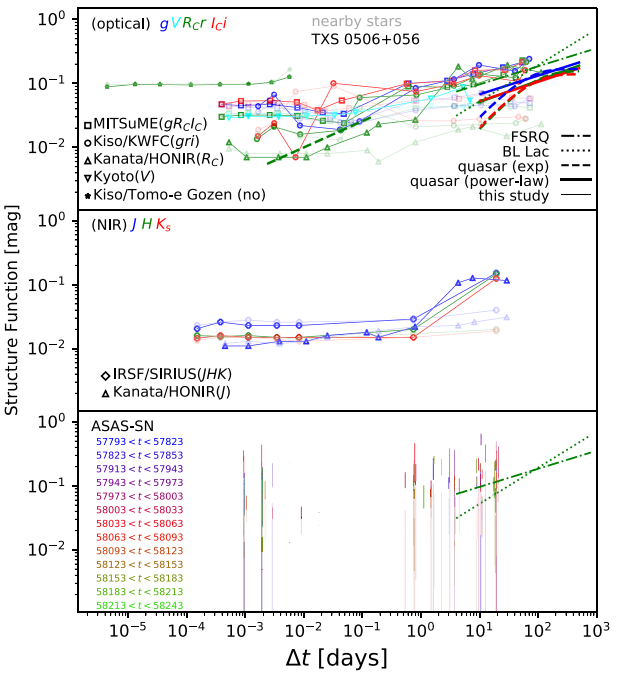

Fig. 5. Optical (top) and NIR (middle) structure functions of TXS 0506+056 obtained in our observations. Power-law and exponential fitting results for quasars (Vanden Berk et al. 2004) are shown in blue (*g*), green (*r*), and red (*i*) thick solid and dashed lines for $\Delta t > 10^1$ d, respectively. Power-law fitting results for FSRQs and BL Lacs (Bauer et al. 2009) are also shown in green dot-dashed and dotted lines, respectively. The flat parts at short time scales are dominated by measurement errors and the real SF amplitudes are thought to be lower than these lines. The optical ASAS-SN structure function as a function of period (every 30 d) is also shown in the bottom panel. (Color online)

the SFs marginally indicate that long-term (10 d) variability around $\sim$60 d before the neutrino detection is the largest, and larger than that in the detection period with a significance of 2.1 σ. On the other hand, the short-term (1 d) variabilities are constant in time. This might indicate that the neutrino emission could be related to the 10 d-timescale variability in this epoch. The hard γ-ray fluxes are also highly variable around this epoch (figure 4).

The correlation between the hard γ-ray fluxes (800 MeV–10 GeV) and optical brightness is investigated in figure 6. The optical magnitudes (brightness) are negatively (positively) correlated with the γ-ray fluxes with Spearman rank correlation coefficients of −0.471 and p-values of <0.03. This indicates that the correlation is significant and TXS 0506+056 is brighter in optical in brighter γ-ray phases, which is consistent with the general trend of ISPs or all types of blazars (Itoh et al. 2016; Jermak et al. 2016).

3.3.2 Intranight variability

Over 22 nights we contiguously took imaging data of TXS 0506+056 for a few tens of minutes or longer with the 0.4 m Kyoto University telescope, MITSuME, Kanata/HONIR, and IRSF/SIRIUS. With these datasets, intranight variability can be investigated.

Magnified views of the light curves on these densely observed nights are shown in the first (optical) and third (NIR) rows of figure 7. In this figure, photometry is performed for each frame. For a comparison, ensemble relative light curves of nearby stars with similar brightness on

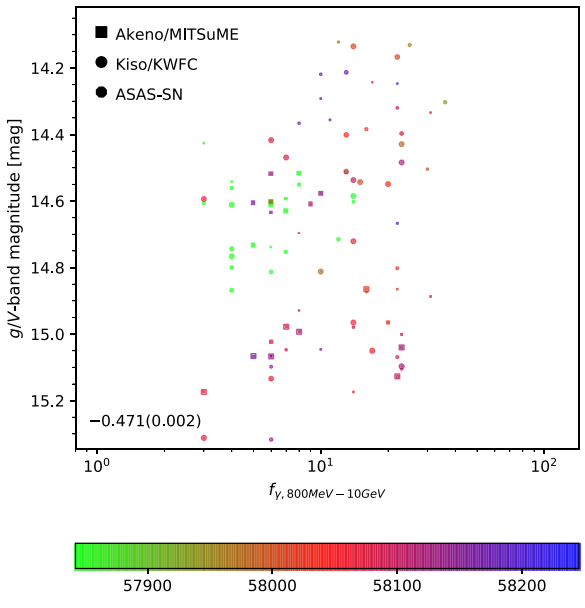

Fig. 6. *g*- or *V*-band magnitude as a function of γ-ray flux. The colors of the points indicate the observing epochs (MJD), as shown in the color bar. (Color online)

average are also shown in the second (optical) and fourth (NIR) rows of the figure. As seen in the daily light curves in figure 4, a brightness change from night to night is easily seen. The root mean square of the brightness is also shown in the figure.

The observed intranight variabilities are as small as 0.03–0.11 mag, depending on the epochs (the data quality), and no significant intranight variabilities are detected in our dataset. The large scatters ($\gtrsim$0.05 mag) seen in some panels of the figure are partly attributed to bad seeing. In Sagar et al. (2004), a few to 10% amplitude ($\lesssim$0.1 mag, 14.1% at maximum) intranight *R*-band variability is seen for 11 blazars (6 BL Lacs and 5 radio core-dominated quasars). The typical observation duration in a night in Sagar et al. (2004) was 6.5 hr and the total number of the observed nights was 47. They found that a duty cycle of intranight optical variability is ∼60% for BL Lacs. Similarly, Paliya et al. (2017) also monitored 17 blazars for 137 hr in the *R* band and also obtained a high duty cycle of ∼40% for blazars. Compared with these studies, the total

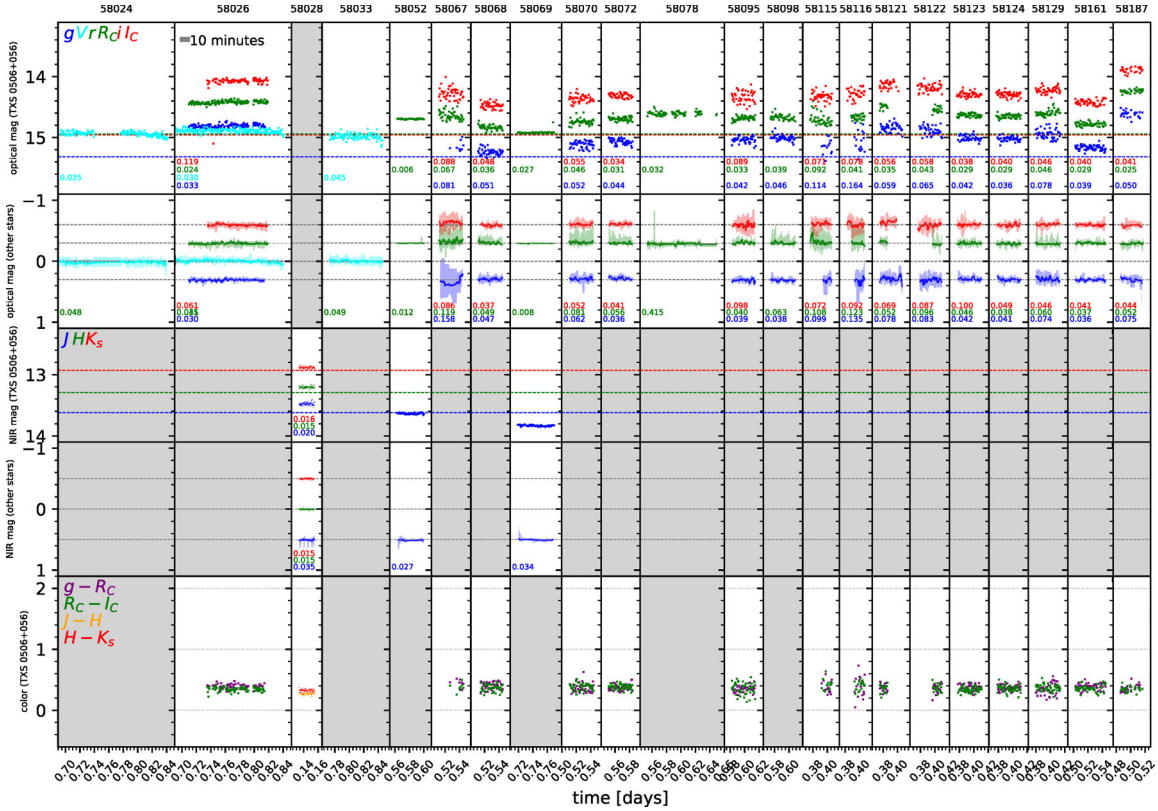

Fig. 7. Light curves of TXS 0506+056 based on photometry for each frame. From top to bottom: optical light curves of TXS 0506+056, optical light curves of nearby similarly bright stars, NIR light curves of TXS 0506+056, NIR light curves of nearby similarly bright stars, and optical and optical–NIR colors of TXS 0506+056. The dates in MJD for the data are shown at the top of each column. The colors used for the optical photometry are blue for *g*, cyan for *V*, green for *R* and *r*, and red for *I* and *i*. The colors used for the NIR photometry are blue for *J*, green for *H*, and red for *K*. The standard deviations in mag within a time window are shown at the bottom left of the panels. The optical PS1 photometry in *gri* bands and NIR 2MASS photometry in JHK_s bands are shown by dashed lines. The thick gray line in the second top panel shows a length of 10 min. Panels with no data are hatched in gray. Large scatters ($\gtrsim$0.05 mag) are partly attributed to bad seeing. (Color online)

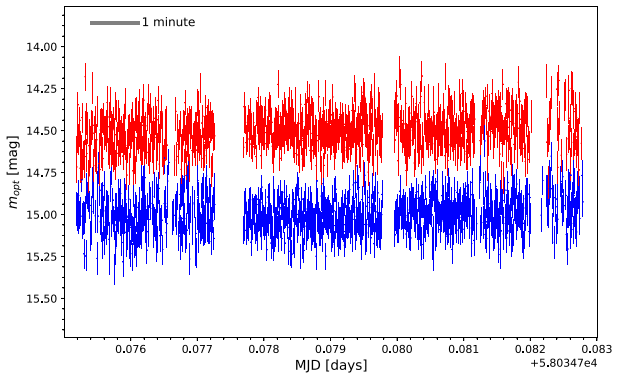

Fig. 8. Optical light curves of TXS 0506+056 (red) and a nearby star (blue) taken with Tomo-e Gozen. (Color online)

duration (sum) of our observations shown in figure 7 is ∼18 hr, and is much shorter by factor of ∼17 (Sagar et al. 2004) and ∼8 (Paliya et al. 2017). It is therefore difficult to see any consistency in our non-detection with these two observations.

3.3.3 Second-scale variability

The fastest variability detected for blazars so far is a few minutes in optical (Sasada et al. 2008) and γ-ray (Albert et al. 2007; Aharonian et al. 2007; Vovk & Neronov 2013; Vovk & Babić 2015; Ackermann et al. 2016), which corresponds to a comparable size of black hole, which indicates a small emitting region in a relativistic jet. The mass of a black hole hosting a blazar is expected to be as much as $\sim 10^9\,M_\odot$ in general (Castignani et al. 2013), and the black hole mass of TXS 0506+056 is estimated to be $\sim 3 \times 10^8\,M_\odot$ (Padovani et al. 2019) by assuming the typical host galaxy luminosity of blazars (Paiano et al. 2018) and the black hole mass and bulge mass relation (McLure & Dunlop 2002). Detection of variability in a shorter time scale would put a tight constraint on the size of an emitting region with the usually assumed Doppler boosting factor. If second-scale variability was detected, this might be attributed to an apparent change in viewing angle to a bent relativistic jet (Raiteri et al. 2017).

Second-scale variability is investigated with the 2 fps Tomo-e Gozen data. Four sets of 180 s (360 frames) exposure were obtained. Detection of TXS 0506+056 was sometimes marginal and we use only photometric data with signal-to-noise ratios of $>10\,\sigma$. As a result, the photometric data in the last (fourth) exposure are partly removed in our analysis and shown in figure 8. The resultant SF is shown in the leftmost part of the top panel of figure 5. In our dataset, no significant rapid variability in the second time scale is detected.

3.4 Optical and NIR colors of TXS 0506+056

Temporal changes of optical, optical–NIR, NIR–NIR colors are shown in figure 4 (entire light curves), figure 7 (intranight light curves), and figure 9 (correlation between magnitudes and colors).

The range of the optical colors of $g - r$ and $g - R$ is 0.2–0.5 mag. A bluer-when-brighter trend is seen in the color–magnitude diagrams (figure 9). This is consistent with the idea that TXS 0506+056 is a BL Lac-type blazar with little contribution from its accretion disk to optical–NIR emission (Bonning et al. 2012). In figure 9, the bluish data points indicating data obtained around MJD = 58200 are offset by ∼0.4 mag from the most crowded (reddish) data region. These bluish data also follow a tighter blue-when-brighter trend. In summary, data points in different epochs follow different color–magnitude relations. This behavior is also observed for other blazars, for example OJ 287, and indicates different activity states between the different loci in the color–magnitude diagram in different epochs (Bonning et al. 2012). These bluish points are data taken after the γ-ray flare in 2018 March (Ojha & Valverd 2018), while the reddish points are taken after the IceCube neutrino detection (IceCube Collaboration 2018). In these two epochs, increased γ-ray fluxes are detected with Fermi but the optical and NIR color–magnitude relations are different from each other. In general, the brighter locations of the bluish points at a given color may be attributed to high-energy electron injection into the jet-emitting region or the emergence of a much brighter accretion disk than usual, possibly due to an accretion state change. Bluer-when-brighter trends of BL Lacs are sometimes attributed to the presumption that the objects are in the high state (Zhang et al. 2015). TXS 0506+056 may show this trend in any state considering that almost featureless power-law continua are always observed and that the equivalent widths (EWs) of the emission lines of TXS 0506+056 ($\mathrm{EW}_{[\mathrm{O\,III}]} = 0.17$ Å at most; Paiano et al. 2018) are small compared to previously measured EWs of blazars (although many of these measurements are upper limits; Landt et al. 2004).

The range of $r - J$ or $R_\mathrm{C} - J$ colors of TXS 0506+056 is from 0.9 to 1.2 (figure 9), roughly corresponding to 1.8 to 2.1 in the Vega system. The $r - J$ and $R_\mathrm{C} - J$ color changes are as small as ∼0.3 mag. Although the previous studies examined different colors (e.g., $V - J$ colors in Ikejiri et al. 2011), these are typical for ISP blazars. The bluer-when-brighter trend is also seen. Note that no data points are shown in the panel of figure 9 after the γ-ray flare in 2018 March reported by Ojha and Valverd (2018).

Intranight changes in optical colors are shown in the bottom panels of figure 7. The $g - r$ or $g - R_\mathrm{C}$ colors are almost constant, about 0.4 mag over all the

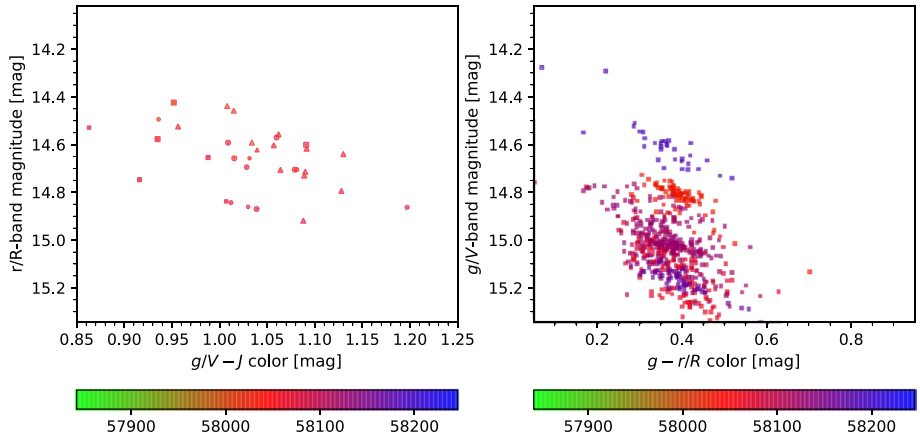

Fig. 9. Optical magnitudes (r or R in the left panel and g or V in the right panel) as functions of optical–NIR color (left panel, $g - J$ or $V - J$) and optical color (right panel, $g - r$ or $g - R$). (Color online)

Table 4. Polarization measurements of TXS 0506+056 with Kanata/HONIR.

		Polarization degree		Polarization angle		
Date (UT)	MJD	R	J	R	J	Note
2017-09-30	58026.771	7.61 ± 0.49	—	24.78 ± 2.65	—	
2017-10-26	58052.770	2.42 ± 0.39	—	17.71 ± 5.54	—	
2017-10-29	58055.736	6.87 ± 1.09	—	10.05 ± 4.94	—	
2017-11-09	58066.790	4.32 ± 0.36	4.47 ± 0.78	16.19 ± 2.47	19.70 ± 2.66	
2017-11-16	58073.761	6.21 ± 2.92	—	30.11 ± 2.37	—	
2018-03-14	58192*	∼14	—	—	—	R, I bands (Steele et al. 2018)
2018-03-22	58199.463	1.50 ± 0.67	3.13 ± 1.22	84.23 ± 12.91	65.33 ± 14.21	
2018-03-24	58201.468	5.90 ± 1.79	—	54.72 ± 9.41	—	
2018-03-25	58202.466	6.59 ± 2.07	—	49.79 ± 11.90	—	
2018-03-26	58203.454	7.20 ± 1.47	7.47 ± 0.61	37.60 ± 2.15	45.62 ± 3.28	
2018-03-27	58204.462	8.01 ± 2.30	—	27.21 ± 2.87	—	
2018-03-28	58205.451	8.58 ± 0.53	7.76 ± 1.52	21.56 ± 1.33	35.36 ± 2.88	
2018-03-31	58208.469	10.15 ± 1.33	11.84 ± 1.75	47.04 ± 1.90	45.86 ± 3.29	
2018-04-02	58210.451	16.99 ± 0.47	—	40.55 ± 0.35	—	
2018-04-03	58211.464	18.88 ± 0.76	16.27 ± 0.78	46.17 ± 2.13	43.91 ± 1.65	
2018-04-08	58216.451	19.26 ± 1.36	20.49 ± 4.59	29.69 ± 1.90	32.63 ± 2.48	
2018-04-09	58217.464	10.47 ± 0.40	8.80 ± 1.33	40.74 ± 3.88	31.69 ± 1.46	
2018-04-13	58221.469	7.23 ± 0.51	—	56.48 ± 2.01	—	

*Calculated by assuming the observations are performed at UT = 0 hr.

nights. The NIR colors of $J - H$ and $H - K$ are also almost constant in time, 0.3–0.4 mag. Note that no significant intranight variability in any band is detected (sub-subsection 3.3.2).

3.5 Polarization of TXS 0506+056

3.5.1 Temporal changes in polarization

Our measurement results for polarization in the R and J bands are summarized in table 4, including the optical polarimetric measurement taken with RINGO3 on the 2 m Liverpool telescope (Steele et al. 2018). The temporal changes of the polarization degrees and angles are shown in figure 4.

For the first five data points taken within 1.5 months of the alert (defined as "first epoch"), the polarization degrees are as small as 2%–8%, as partly reported in Yamanaka et al. (2017). About 6 months after the neutrino detection (defined as "second epoch"), Ojha and Valverd (2018) reported that a flare of the highest daily averaged γ-ray flux for TXS 0506+056 was detected with Fermi on 2018 March 13. Soon after that, Steele, Jermak, and

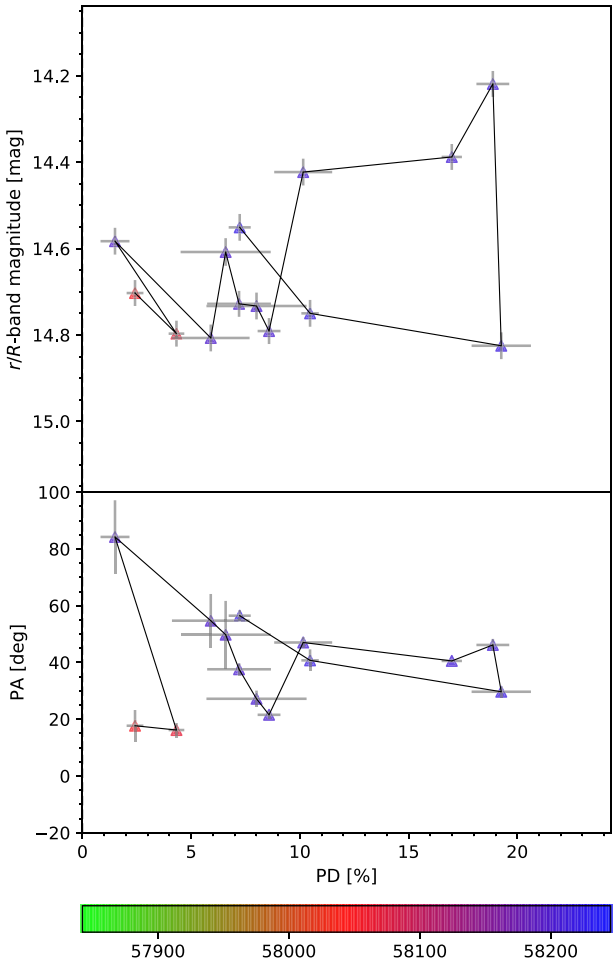

Fig. 10. The *r*- or *R*-band magnitude and *R*-band polarization angle as a function of the *R*-band polarization degree. All the data points are connected in time sequence. The different symbols indicate data taken with different telescopes/instruments in the same way as in figure 4. (Color online)

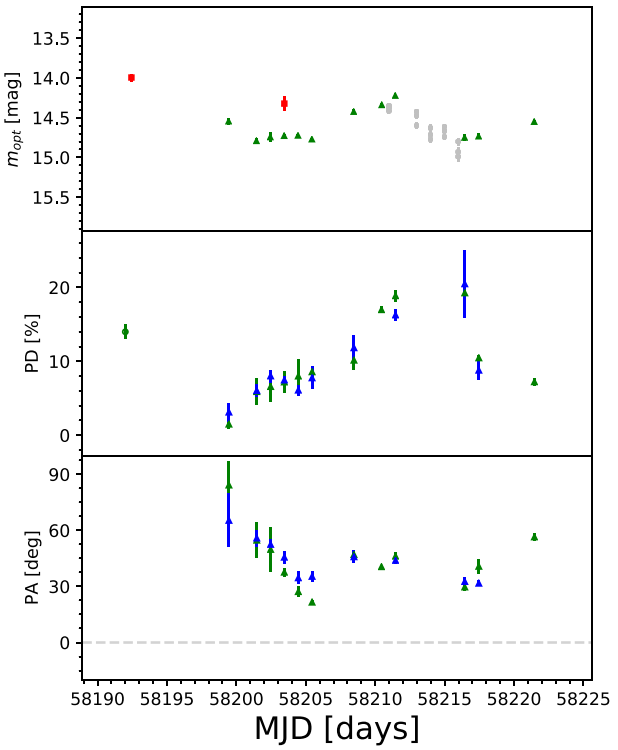

Fig. 11. Magnified view of temporal changes of optical magnitudes, polarization degrees, and polarization angles around the γ-ray flare reported by Ojha and Valverd (2018). The symbols and colors are the same as in figure 4. (Color online)

Copperwheat (2018) carried out polarimetric observation on the night of 2018 March 14 with Liverpool/RINGO3 and found that the optical polarization degree increases up to ∼14% at wavelengths roughly corresponding to the *R* and *I* bands. As shown in figure 4 and table 4, our subsequent observations with Kanata/HONIR (12 polarization measurements for 23 d starting 8 d after the RINGO3 observation) indicate that the optical polarization degree again decreases down to 1.5% on March 22, which is even lower than the observed level in the first epoch. After this decrease, the polarization degrees gradually increase up to ∼20% over about two weeks and then decrease again down to 7.2%, which is as low as those in the first epoch. Throughout this period, the *J*-band polarization exhibits a similar time variation behavior to the *R* band.

In ISPs, typical polarization degrees and their temporal change are ∼30% and ∼20% or less, respectively, among the samples observed by Ikejiri et al. (2011), Itoh et al. (2016), and Jermak et al. (2016). The polarization degrees and the temporal change observed in TXS 0506+056 is comparable to or less than these, being consistent with those objects.

The polarization angles are roughly constant at $\sim 20^\circ \pm 10^\circ$ in both *R* and *J* bands in the first epoch. In the second epoch, our HONIR measurements indicate that the polarization angles are 20°–90° and significantly different from those in the first epoch. Following the polarization degree increase from 1.5% to ∼20%, the polarization angles first change from 84° to 22° and then back to 30°–60°. The position angles in the *J* band also show a similar behavior to the *R* band.

3.5.2 Correlations between optical brightness and polarization

The top panel of figure 10 shows the relation between the polarization degrees and optical *r*- or *R*-band magnitudes. Although the optical brightness and polarization degrees look roughly coincident with each other as a whole (figure 4), almost no correlations are seen during the rapid changes in the second epoch, as indicated by the bluish points in figure 10. This is discussed later in this subsection.

Polarization changes in optical wavelengths associated with γ-ray flares are reported in the literature (Sasada et al.

2008; Abdo et al. 2010). In the second epoch, the polarization change of TXS 0506+056 seems to be associated with the γ-ray flare (Ohja & Valverd 2018), although such correlated behavior is not clear in the first epoch because the polarization measurements were not performed right after (or before) the neutrino detection, the measurements are sparse, and the number of measurements is small. In Itoh et al. (2013), no brightness flare was observed during their first polarization flare for the famous blazar CTA 102 (an FSRQ at $z = 1.037$), indicating that the polarization degree does not necessarily correlate with brightness.

The lack of strong correlations between optical brightness and polarization degree in our data for TXS 0506+056 is similarly observed in previous works on other blazars (Ikejiri et al. 2011; Jermak et al. 2016), although a significant negative (positive) correlation between "amplitudes" of flux and polarization degree is detected for two blazars (AO 0235+164 and PKS 1510−089) over a 10 d time scale (Sasada et al. 2011). These observed weak correlations could be partly due to ignorance of a possible time lag between temporal changes of fluxes and polarization degrees (Uemura et al. 2017). Figure 11 is a magnified view of figure 4 around the second epoch. The peak of the polarization degrees is around MJD∼58211–58217 d, while that of optical brightness is around MJD∼58210–58211 d. This indicates that the optical brightness change precedes the polarization degree change, which is the opposite sense to that observed for the BL Lac PKS 1749+096 as reported by Uemura et al. (2017). This lag partly makes the correlation worse in figure 10. A positive correlation would be seen if the data point in MJD = 58217 (the bottom right point in figure 10) is ignored.

The polarization angles also change in time by $\sim 70^{\circ}$ in the second epoch, although the change is not so drastically large. Figure 11 indicates that the polarization angles decrease as the polarization degrees increase in the period MJD = 58198–58207. The polarization degrees still increase after that, but the polarization angles do not show a systematic decrease. These make the correlation between the polarization angles and degrees poor, as shown in the bottom panel of figure 10. Changes of polarization angles are observed for many blazars (Itoh et al. 2016; Hovatta et al. 2016). The observed change of the polarization angles for TXS 0506+056 is not so large, which is sometimes explained by a curved structure of a relativistic jet (Abdo et al. 2010; Sorcia et al. 2014).

3.6 Spectra of TXS 0506+056

All of our three new spectra of TXS 0506+056 are shown in figure 12. The Subaru/FOCAS spectra in the two different setups shown in IceCube Collaboration (2018) are also plotted as references. All these spectra were taken in roughly similar epochs, ∼1 week to ∼1.5 months after the neutrino detection, and before the GTC/OSIRIS spectrum, which conclusively determines the redshift of TXS 0506+056, was taken (Paiano et al. 2018). In the epochs of our observations, TXS 0506+056 is slightly brighter ($g = 14.8$–15.1) than in the GTC observation ($g = 15.4$; Paiano et al. 2018), which makes line detections more difficult. All of our three spectra show basically featureless continua and no significant emission or absorption lines are detected, except for the weak emission line in the Subaru/FOCAS spectrum (IceCube Collaboration 2018). These are quantitatively consistent with the spectrum of Paiano et al. (2018). No significant changes between the different epochs were detected.

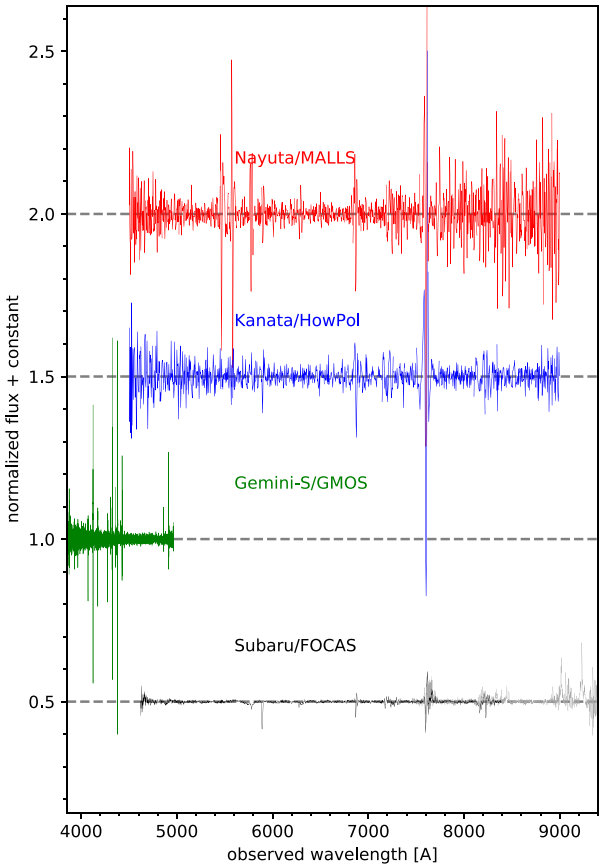

Fig. 12. Optical spectra of TXS 0506+056 taken with Nayuta/MALLS (red), Kanata/HOWPol (blue), Gemini-South/GMOS (green), and Subaru/FOCAS (black). The Subaru/FOCAS spectra are the same as those shown in IceCube Collaboration (2018). There are no changes in spectral features. Noisy wavelength ranges are omitted. The spiky features seen in the spectra are all atmospheric. (Color online)

4 Summary

We first made optical and NIR imaging observations to search for a candidate for the neutrino source of IceCube-170922A. We found that TXS 0506+056 was

rapidly fading in NIR over a day scale. Motivated by this discovery of rapid NIR variability, a γ-ray flare was discovered in the Fermi/LAT monitoring data. We conducted monitoring observations of TXS 0506+056 with Akeno/MITSuME, Kiso/KWFC, Kiso/Tomo-e Gozen, Kyoto 0.4 m, Kanata/HONIR, and Subaru/HSC. Polarization imaging data were also taken with Kanata/HONIR at 17 epochs. We also took optical spectra four times with Kanata/HOWPol, Nayuta/MALLS, Gemini-N/GMOS, and Subaru/FOCAS.

Combining this data with ASAS-SN optical monitoring data and Fermi/LAT γ-ray data, we find:

- daily variability is significant and as large as 1.0 mag;
- no significant intranight variability is detected;
- no special optical/NIR variability behavior was detected over the observed period, but there was a very marginal sign of a larger variability over a time scale of $\sim$10 d about 2 months before the neutrino detection;
- weak correlation between optical/NIR and γ-ray fluxes;
- large changes in polarization degrees and angles about 180 d after the neutrino detection;
- weak or no correlation between polarization degree and optical fluxes, while some correlated behavior can be seen in part of the 2018 March ($\sim$180 d after the neutrino detection) data;
- no significant optical spectral changes over the three months after the neutrino detection.

In summary, our data do not indicate that TXS 0506+056 is a special blazar (BL Lac) among other blazars in terms of intranight, daily, monthly optical/NIR variability, and optical polarization. The neutrino detection is also not a special timing.

For future Icecube neutrino events, to further examine possible relations between high-energy neutrinos and blazars, as well as blazar variability, more complete blazar catalogs like the recently developed BROS (Itoh et al. 2020) are required. In addition, in optical and NIR wavelengths, routine high-cadence imaging and polarization monitoring of blazars are desired. Normal imaging observations are done in several wide-field surveys such as the Zwicky Transient Facility (ZTF; Graham et al. 2019) and Tomo-e Gozen (Sako et al. 2018). Polarization monitoring is a more expensive observation program but is expected to provide unique science outputs.

Acknowledgment

Observations with the Kanata, Nayuta, MITSuME, and Kiso Schmidt telescopes were supported by the Optical and Near-infrared Astronomy Inter-University Cooperation Program and Grants-in-Aid of the Ministry of Education, Science, Culture, and Sport Nos. JP23740143, JP25800103, JP16H02158, JP18H04575, JP15H02075, JP16H06341, JP18H05223, JP17K14253, JP17H04830, JP26800103, JP19H00693, JP17H06363, JP17H06362, JP24103003, JP1805458, and JP19K14772.

This work was partly supported by the joint research program of the Institute for Cosmic Ray Research (ICRR), National Astronomical Observatory of Japan (NAOJ), and JSPS and National Science Foundation (NSF) under the JSPS-NSF Partnerships for International Research and Education (PIRE). This work was also based in part on data collected at the Subaru Telescope, which is operated by the National Astronomical Observatory of Japan. Based on observations obtained at the international Gemini Observatory, a program of NOIRLab, which is managed by the Association of Universities for Research in Astronomy (AURA) under a cooperative agreement with the National Science Foundation. on behalf of the Gemini Observatory partnership: the National Science Foundation (United States), National Research Council (Canada), Agencia Nacional de Investigación y Desarrollo (Chile), Ministerio de Ciencia, Tecnología e Innovación (Argentina), Ministério da Ciência, Tecnologia, Inovações e Comunicações (Brazil), and the Korea Astronomy and Space Science Institute (Republic of Korea).

The IRSF project is a collaboration between Nagoya University and the SAAO supported by Grants-in-Aid for Scientific Research on Priority Areas (A) (nos. 10147207 and 10147214) and the Optical & Near-Infrared Astronomy Inter-University Cooperation Program from the Ministry of Education, Culture, Sports, Science and Technology (MEXT) of Japan and the National Research Foundation (NRF) of South Africa.

The Pan-STARRS1 Surveys (PS1) and the PS1 public science archive have been made possible through contributions by the Institute for Astronomy, the University of Hawaii, the Pan-STARRS Project Office, the Max-Planck Society and its participating institutes, the Max Planck Institute for Astronomy, Heidelberg and the Max Planck Institute for Extraterrestrial Physics, Garching, The Johns Hopkins University, Durham University, the University of Edinburgh, the Queen's University Belfast, the Harvard-Smithsonian Center for Astrophysics, the Las Cumbres Observatory Global Telescope Network Incorporated, the National Central University of Taiwan, the Space Telescope Science Institute, the National Aeronautics and Space Administration under Grant No. NNX08AR22G issued through the Planetary Science Division of the NASA Science Mission Directorate, the National Science Foundation Grant No. AST-1238877, the University of Maryland, Eotvos Lorand University (ELTE), the Los Alamos National Laboratory, and the Gordon and Betty Moore Foundation.

This publication makes use of data products from the Two Micron All Sky Survey, which is a joint project of the University of Massachusetts and the Infrared Processing and Analysis Center/California Institute of Technology, funded by the National Aeronautics and Space Administration and the National Science Foundation.

The data is partly processed using the Gemini IRAF package. The authors acknowledge Dr. N. Matsunaga for software to conduct comparisons between our image coordinates and the catalog values.

References

Aartsen, M. G., et al. 2014, Phys. Rev. Lett., 113, 101101
Aartsen, M. G., et al. 2015, ApJ, 811, 52
Aartsen, M. G., et al. 2017a, ApJ, 835, 45
Aartsen, M. G., et al. 2017b, ApJ, 843, 112
Aartsen, M. G., et al. 2017c, Astropart. Phys., 92, 30

Abdo, A. A., et al. 2010, Nature, 463, 919
Abdollahi, S., et al. 2017, ApJ, 846, 34
Ackermann, M., et al. 2016, ApJ, 824, L20
Aharonian, F., et al. 2007, ApJ, 664, L71
Ajello, M., et al. 2014, ApJ, 780, 73
Akitaya, H., et al. 2014, Proc. SPIE, 9147, 91474O
Alard, C. 2000, A&AS, 144, 363
Alard, C., & Lupton, R. H. 1998, ApJ, 503, 325
Albert, J., et al. 2007, ApJ, 669, 862
Ansoldi, S., et al. 2018, ApJ, 863, L10
Bachev, R., et al. 2017, MNRAS, 471, 2216
Baltay, C., et al. 2007, PASP, 119, 1278
Bauer, A., Baltay, C., Coppi, P., Ellman, N., Jerke, J., Rabinowitz, D., & Scalzo, R. 2009, ApJ, 699, 1732
Bechtol, K., Ahlers, M., Di Mauro, M., Ajello, M., & Vandenbroucke, J. 2017, ApJ, 836, 47
Becker, J. K., Biermann, P. L., & Rhode, W. 2005, Astropart. Phys., 23, 355
Bertin, E., & Arnouts, S. 1996, A&AS, 117, 393
Bonning, E., et al. 2012, ApJ, 756, 13
Bosch, J., et al. 2018, PASJ, 70, S5
Castignani, G., Haardt, F., Lapi, A., De Zotti, G., Celotti, A., & Danese, L. 2013, A&A, 560, A28
Chambers, K. C., et al. 2016, arXiv:1612.05560
Condon, J. J., Cotton, W. D., Greisen, E. W., Yin, Q. F., Perley, R. A., Taylor, G. B., & Broderick, J. J. 1998, AJ, 115, 1693
de Gasperin, F., Intema, H. T., & Frail, D. A. 2018, MNRAS, 474, 5008
de Naurois, M. H. E. S. S. Collaboration 2017, Astronomer's Telegram, 10787
Dingus, B. L., & Bertsch, D. L. 2001, in AIP Conf. Ser., 587, Gamma 2001: Gamma-Ray Astrophysics, ed. S. Ritz et al. (New York: AIP), 251
Dornic, D., & Coleiro, A. 2017a, GCN Circ., 21923, 1
Dornic, D., & Coleiro, A. 2017b, Astronomer's Telegram, 10773
Douglas, J. N., Bash, F. N., Bozyan, F. A., Torrence, G. W., & Wolfe, C. 1996, AJ, 111, 1945
Eichler, D. 1979, ApJ, 232, 106
Emmanoulopoulos, D., McHardy, I. M., & Uttley, P. 2010, MNRAS, 404, 931
Flewelling, H. A., et al. 2016, arXiv:1612.05243
Fossati, G., Maraschi, L., Celotti, A., Comastri, A., & Ghisellini, G. 1998, MNRAS, 299, 433
Franckowiak, A., Stanek, K. Z., Kochanek, C. S., Thompson, T. A., Holoien, T. W. S., Shappee, B. J., Prieto, J. L., & Dong, S. 2017, Astronomer's Telegram, 10794
Gaur, H., Gupta, A., Bachev, R., Strigachev, A., Semkov, E., Wiita, P., Gu, M., & Ibryamov, S. 2017, Galaxies, 5, 94
Ghisellini, G., Righi, C., Costamante, L., & Tavecchio, F. 2017, MNRAS, 469, 255
Graham, M. J., et al. 2019, PASP, 131, 078001
Halpern, J. P., Eracleous, M., & Mattox, J. R. 2003, AJ, 125, 572
Henden, A., & Munari, U. 2014, Contrib. Astron. Obs. Skalnaté Pleso, 43, 518
Hook, I. M., Jørgensen, I., Allington-Smith, J. R., Davies, R. L., Metcalfe, N., Murowinski, R. G., & Crampton, D. 2004, PASP, 116, 425
Hovatta, T., et al. 2016, A&A, 596, A78
IceCube Collaboration 2015, arXiv:1510.05223
IceCube Collaboration 2017, A&A, 607, A115
IceCube Collaboration 2018, Science, 361, eaat1378
Ikejiri, Y., et al. 2011, PASJ, 63, 639
Inoue, Y., Khangulyan, D., Inoue, S., & Doi, A. 2019, ApJ, 880, 40
Intema, H. T., Jagannathan, P., Mooley, K. P., & Frail, D. A. 2017, A&A, 598, A78
Itoh, R., et al. 2013, ApJ, 768, L24
Itoh, R., et al. 2016, ApJ, 833, 77
Itoh, R., et al. 2017, PASJ, 69, 25
Itoh, R., Utsumi, Y., Inoue, Y., Ohta, K., Doi, A., Morokuma, T., Kawabata, K. S., & Tanaka, Y. T. 2020, ApJ, 901, 3
Jermak, H., et al. 2016, MNRAS, 462, 4267
Kadler, M., et al. 2016, Nature Phys., 12, 807
Kashikawa, N., et al. 2002, PASJ, 54, 819
Kawabata, K. S., et al. 1999, PASP, 111, 898
Keivani, A., Evans, P. A., Kennea, J. A., Fox, D. B., Cowen, D. F., Osborne, J. P., & Marshall, F. E. 2017, GCN Circ., 21930, 1
Kochanek, C. S., et al. 2017, PASP, 129, 104502
Kojima, Y., et al. 2018, Proc. SPIE, 10709, 107091T
Kopper, C., & Blaufuss, E. 2017, GCN Circ., 21916
Kostov, A., & Bonev, T. 2018, Bulgarian Astron. J., 28, 3
Kotani, T., et al. 2005, Nuovo Cim. C, 28, 755
Kotera, K., Allard, D., & Olinto, A. V. 2010, JCAP, 10, 013
Kubo, H., Takahashi, T., Madejski, G., Tashiro, M., Makino, F., Inoue, S., & Takahara, F. 1998, ApJ, 504, 693
Landoni, M., et al. 2015a, AJ, 149, 163
Landoni, M., Falomo, R., Treves, A., Scarpa, R., & Reverte Payá, D. 2015b, AJ, 150, 181
Landt, H., Padovani, P., Perlman, E. S., & Giommi, P. 2004, MNRAS, 351, 83
Lang, D., Hogg, D. W., Mierle, K., Blanton, M., & Roweis, S. 2010, AJ, 139, 1782
Li, X.-P., Yang, H.-Y., Luo, Y.-H., Yang, C., Cai, Y., Yang, H.-T., & Zhang, L. 2018, MNRAS, 479, 4073
Loeb, A., & Waxman, E. 2006, JCAP, 2006, 003
Lucarelli, F., et al. 2019, ApJ, 870, 136
McLure, R. J., & Dunlop, J. S. 2002, MNRAS, 331, 795
Magnier, E. A., et al. 2016, arXiv:1612.05242
Mannheim, K. 1995, Astropart. Phys., 3, 295
Marscher, A. P., & Gear, W. K. 1985, ApJ, 298, 114
Martinez, I., & Taboada, I. 2017, GCN Circ., 21924, 1
Mirzoyan, R. 2017, Astronomer's Telegram, 10817
Mirzoyan, R. 2018, Astronomer's Telegram, 12260
Miyazaki, S., et al. 2012, in Proc. SPIE, 8446, Ground-based and Airborne Instrumentation for Astronomy IV, ed. I. S. McLean et al. (Bellingham, WA: SPIE), 84460Z
Morokuma, T., et al. 2014, PASJ, 66, 114
Morokuma, T., Tanaka, Y. T., Ohta, K., Matsuoka, Y., Yamashita, T., & Kato, N. 2017, Astronomer's Telegram, 10890
Mücke, A., Protheroe, R. J., Engel, R., Rachen, J. P., & Stanev, T. 2003, Astropart. Phys., 18, 593
Murase, K., Ahlers, M., & Lacki, B. C. 2013, Phys. Rev. D, 88, 121301
Murase, K., Thompson, T. A., Lacki, B. C., & Beacom, J. F. 2011, Phys. Rev. D, 84, 043003
Nagayama, T. 2012, African Skies, 16, 98

Nagayama, T., et al. 2003, in Proc. SPIE, 4841, Instrument Design and Performance for Optical/Infrared Ground-based Telescopes, ed. M. Iye & A. F. M. Moorwood (Bellingham, WA: SPIE), 459
Ohsawa, R., et al. 2016, in Proc. SPIE, 9913, Software and Cyberinfrastructure for Astronomy IV, ed. G. Chiozzi & J. C. Guzman (Bellingham, WA: SPIE), 991339
Ojha, R., & Valverd, J. 2018, Astronomer's Telegram, 11419
Padovani, P., Giommi, P., Resconi, E., Glauch, T., Arsioli, B., Sahakyan, N., & Huber, M. 2018, MNRAS, 480, 192
Padovani, P., Oikonomou, F., Petropoulou, M., Giommi, P., & Resconi, E. 2019, MNRAS, 484, L104
Paiano, S., Falomo, R., Treves, A., & Scarpa, R. 2018, ApJ, 854, L32
Paliya, V. S., Stalin, C. S., Ajello, M., & Kaur, A. 2017, ApJ, 844, 32
Raiteri, C. M., et al. 2017, Nature, 552, 374
Rani, B., Gupta, A. C., Joshi, U. C., Ganesh, S., & Wiita, P. J. 2011, MNRAS, 413, 2157
Razzaque, S., Mészáros, P., & Waxman, E. 2004, Phys. Rev. Lett., 93, 181101
P. J.,Sagar, R., Stalin, C. S., & Gopal-Krishna, Wiita2004, MNRAS, 348, 176
Sako, S., et al. 2012, in Proc. SPIE, 8446, Ground-based and Airborne Instrumentation for Astronomy IV, ed. I. S. McLean et al. (Bellingham, WA: SPIE), 84466L
Sako, S., et al. 2016, in Proc. SPIE, 9908, Ground-based and Airborne Instrumentation for Astronomy VI, ed. C. J. Evans et al. (Bellingham, WA: SPIE), 99083P
Sako, S., et al. 2018, in Proc. SPIE, 10702, Ground-based and Airborne Instrumentation for Astronomy VII, ed. C. J. Evans et al. (Bellingham, WA: SPIE), 107020J
Sandrinelli, A., Covino, S., & Treves, A. 2014, A&A, 562, A79
Sasada, M., et al. 2008, PASJ, 60, L37
Sasada, M., et al. 2011, PASJ, 63, 489
Savchenko, V., Ferrigno, C., Ubertini, P., Bazzano, A., Natalucci, L., Mereghetti, S., Laurent, P., & Kuulkers, E. 2017, GCN Circ., 21917, 1
Schlafly, E. F., & Finkbeiner, D. P. 2011, ApJ, 737, 103
Schmidt, G. D., Elston, R., & Lupie, O. L. 1992, AJ, 104, 1563
Senno, N., Murase, K., & Mészáros, P. 2016, Phys. Rev. D, 93, 083003
Senno, N., Murase, K., & Mészáros, P. 2017, ApJ, 838, 3
Serkowski, K., Mathewson, D. S., & Ford, V. L. 1975, ApJ, 196, 261
Shappee, B. J., et al. 2014, ApJ, 788, 48
Shimokawabe, T., et al. 2008, in AIP Conf. Proc., 1000, Gamma-Ray Bursts 2007, ed. M. Galassi et al. (New York: AIP), 543
Skrutskie, M. F., et al. 2006, AJ, 131, 1163
Sorcia, M., Benítez, E., Hiriart, D., López, J. M., Cabrera, J. I., & Mújica, R. 2014, ApJ, 794, 54
Steele, I. A. 2017, Astronomer's Telegram, 10799
Steele, I. A., Jermak, H., & Copperwheat, C. 2018, Astronomer's Telegram, 11430
Stein, R., et al. 2020, arXiv:2005.05340
Tabur, V. 2007, PASA, 24, 189
Tachibana, Y., et al. 2018, PASJ, 70, 92
Tanaka, Y. T., Buson, S., & Kocevski, D. 2017, Astronomer's Telegram, 10791
Tokunaga, A. T., & Vacca, W. D. 2005, PASP, 117, 421
Uemura, M., et al. 2017, PASJ, 69, 96
Vanden Berk, D. E., et al. 2004, ApJ, 601, 692
Vovk, I., & Babić, A. 2015, A&A, 578, A92
Vovk, I., & Neronov, A. 2013, ApJ, 767, 103
Waxman, E., & Bahcall, J. 1997, Phys. Rev. Lett., 78, 2292
White, G. L., Jauncey, D. L., Savage, A., Wright, A. E., Batty, M. J., Peterson, B. A., & Gulkis, S. 1988, ApJ, 327, 561
Winter, W. 2013, Phys. Rev. D, 88, 083007
Yamanaka, M., Tanaka, Y. T., Mori, H., Kawabata, K. S., Utsumi, Y., Nakaoka, T., Kawabata, M., & Nagashima, H. 2017, Astronomer's Telegram, 10844
Yatsu, Y., et al. 2007, Phys. E, 40, 434
York, D. G., et al. 2000, AJ, 120, 1579
Zhang, B.-K., Zhou, X.-S., Zhao, X.-Y., & Dai, B.-Z. 2015, Res. Astron. Astrophys., 15, 1784